A critical analysis of dipole-moment calculations as obtained from experimental and theoretical structure factors

Agnieszka Poulain-Paul, Ayoub Nassour, Christian Jelsch, Benoit Guillot, Maciej Kubicki, Claude Lecomte

Acta Crystallographica Section A
Foundations of Crystallography
ISSN 0108-7673

Received 6 June 2012
Accepted 30 July 2012

A critical analysis of dipole-moment calculations as obtained from experimental and theoretical structure factors

Agnieszka Poulain-Paul,[a,b] Ayoub Nassour,[a] Christian Jelsch,[a] Benoit Guillot,[a] Maciej Kubicki[b] and Claude Lecomte[a]*

[a]CRM2 UMR CNRS and Lorraine University, BP 70239, 54506 Vandoeuvre-les-Nancy Cedex, France, and [b]Faculty of Chemistry, Adam Mickiewicz University, Grunwaldzka 6, 60-780 Poznań, Poland. Correspondence e-mail: claude.lecomte@crm2.uhp-nancy.fr

Three models of charge-density distribution – Hansen–Coppens multipolar, virtual atom and kappa – of different complexities, different numbers of refined parameters, and with variable levels of restraints, were tested against theoretical and high-resolution X-ray diffraction structure factors for 2-methyl-4-nitro-1-phenyl-1*H*-imidazole-5-carbonitrile. The influence of the model, refinement strategy, multipole level and treatment of the H atoms on the dipole moment was investigated. The dipole moment turned out to be very sensitive to the refinement strategy. Also, small changes in H-atom treatment can greatly influence the calculated magnitude and orientation of the dipole moment. The best results were obtained when H atoms were kept in positions determined by neutron diffraction and anisotropic displacement parameters (obtained by *SHADE*, in this case) were used. Also, constraints on kappa values of H atoms were found to be superior to the free refinement of these parameters. It is also shown that the over-parametrization of the multipolar model, although possibly leading to better residuals, in general gives worse dipole moments.

1. Introduction

The extraction of reproducible and reliable electrostatic properties from a charge-density analysis is a key issue in assessing the physical reliability of experimental diffraction data refinement. The multipolar modelling may be influenced by many factors, such as diffraction data quality, thermal smearing or correlations between refined parameters. Even if the electron density is statistically well fitted to the experimental data in the process of refinement, the resulting atomic and molecular properties, for example electrostatic potential, dipole moments ($\boldsymbol{\mu}$) and interaction energies, can be questionable due to the lack of physical constraints (Spackman, 1992; Coppens, 1997; Pérès *et al.*, 1999; Volkov *et al.*, 2001; Spackman *et al.*, 2007; Domagała & Jelsch, 2008 and references therein). Several attempts were made to test various electron-density models, available pseudoatom databases (Durka *et al.*, 2010; Bąk *et al.*, 2011) or the influence of constraints on the electrostatic properties. Using experimental and theoretical data (Abramov *et al.*, 1999; Volkov *et al.*, 2000), it was found, for instance, that the large differences between $\boldsymbol{\mu}$ values observed between multipolar and integrated atom-in-molecules (AIM) (Bader, 1990) methods may be caused by the partitioning method rather than by the differences in charge distribution, choice of the multipole model – unrestricted or κ-restricted (Volkov *et al.*, 2000) – or by the order of multipoles. On the other hand, the dipole moments in crystals derived from multipolar refinements of X-ray data are generally found to be larger than those calculated *ab initio* for the molecule *in vacuo*, due to induced polarization. An increase has also been observed in comparison with the values obtained from theoretical calculations (Abramov *et al.*, 1999).

For the last ten years, we have been investigating the charge-density distribution of a series of nitroimidazole derivatives (Kubicki *et al.*, 2002; Paul, Kubicki, Jelsch *et al.*, 2011; Paul, Kubicki, Kubas *et al.*, 2011). In this last paper (Paul, Kubicki, Kubas *et al.*, 2011) large discrepancies were observed between the dipole moment of 2-methyl-4-nitro-1-phenyl-1*H*-imidazole-5-carbonitrile [compound (I), Fig. 1] calculated from theoretical and experimental data. The theoretical calculations were performed for a single molecule of (I) (B3LYP+D, $\boldsymbol{\mu}$ = 9.68 D) and using a conductor-like screening model (COSMO, $\boldsymbol{\mu}$ = 12.4 D, with the dielectric constant ε set to infinity to mimic the screening of the electrostatic moments in the crystal). The moment derived from experimental diffraction data using the multipolar Hansen–Coppens model was 25.7 D.

The magnitude of the dipole moment obtained from experiment was much higher than that derived from theoretical diffraction data. Furthermore, this dipole moment was found to be extremely dependent on the refinement strategy, which is not the case, for example, when comparing topolo-

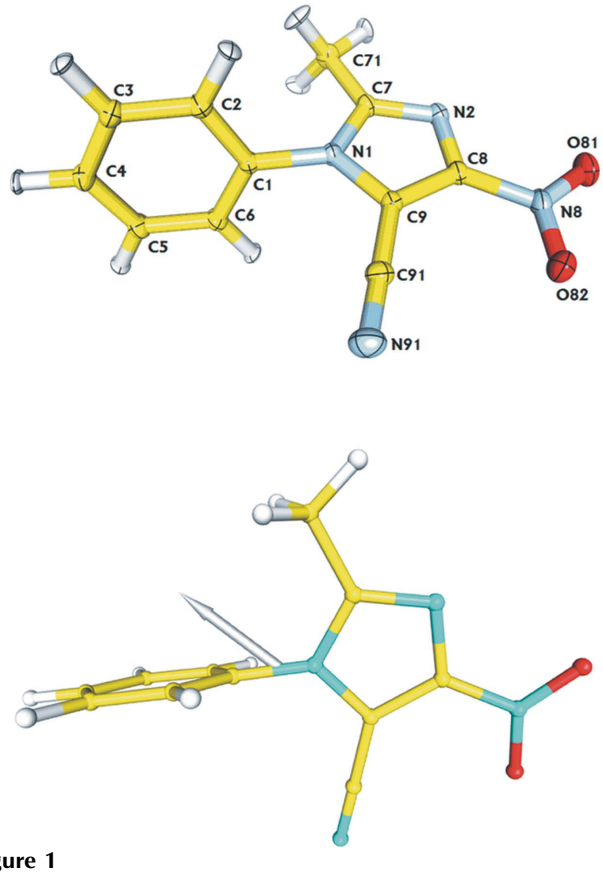

Figure 1
Top: molecule (I) with the atom-labelling scheme (Paul, Kubicki, Kubas *et al.*, 2011). Ellipsoids are drawn at the 50% probability level, H-atom ADPs estimated by *SHADE*. The compound crystallizes in the monoclinic $P2_1/n$ space group, with the unit-cell parameters a = 9.8484 (1), b = 9.3614 (1) , c = 11.6487 (1) Å, β = 103.573 (1)°. Bottom: reference dipole vector from *CRYSTAL09*.

gical properties. Therefore, we decided to analyse various models based on theoretical and experimental data for compound (I) in order to assess the reliability of the refinement and to find the best model for calculation of the electronic properties. It is also desirable, for instance, for applications to macromolecules (proteins, nucleic acids), to find the simplest model that would be able to describe accurately the electrostatic characteristics of the molecule. The chosen molecule (Fig. 1, top) seems to be especially suitable for such investigation, because it has two strongly electronegative (cyano and nitro) groups on one side and all H atoms are located on the other side. Hence it is known that: (*a*) dipole moments are generally affected by intermolecular electrostatic interactions and molecules tend to line up in a crystal to maximize the electrostatic attractions (Abramov *et al.*, 1999 and references therein); (*b*) treatment of peripheral H atoms plays a significant role in determining electrostatic properties (Spackman *et al.*, 2007).

The aim of this paper is to propose a strategy for estimating reliable molecular dipole moments from X-ray charge-density refinements. At first, for the molecular crystal of (I), a set of theoretical structure factors up to s = 1.2 Å^{-1} reciprocal resolution was generated with the *CRYSTAL09* package (Dovesi *et al.*, 2010) based on density functional theory (DFT) (Hohenberg & Kohn, 1964) at the B3LYP level with the 6-31G(d,p) basis set (Hariharan & Pople, 1973) and three charge-density models have been applied to these data (details of the models used are given in §2):

(i) Hansen–Coppens (Hansen & Coppens, 1978) multipolar atom model as coded in the software *MoPro* (Jelsch *et al.*, 2005).

(ii) Spherical virtual-atom refinement (Dadda *et al.*, 2012).

(iii) Spherical atom kappa refinement (Coppens *et al.*, 1979).

For each of these crystallographic refinements, several strategies were applied (H-atom modelling, constraints, restraints, order of multipolar modelling). The resulting molecular dipole moments were compared to the theoretical one ($\boldsymbol{\mu}$ = 10.6 D) calculated directly with *CRYSTAL09* in the crystalline state ($\boldsymbol{\mu}$ calculated for a single molecule in *CRYSTAL09* is 9.2 D). Then, a refinement strategy was proposed and applied to the experimental diffraction data.

2. Methods

2.1. Theoretical structure-factor generation

Periodic quantum-mechanical calculations using *CRYSTAL09* (Dovesi *et al.*, 2010) were performed at the optimized geometry starting from the experimental crystal structure (Paul, Kubicki, Kubas *et al.*, 2011) with the DFT method (Hohenberg & Kohn, 1964) and with the B3LYP hybrid functional (Lee *et al.*, 1988) using the 6-31G(d,p) basis set (Hariharan & Pople, 1973). The level of accuracy in evaluating the Coulomb and exchange series is controlled by five parameters for which the values of 10^{-6}, 10^{-6}, 10^{-6}, 10^{-6} and 10^{-17} were used. The shrinking factor of the reciprocal space was set to 4, corresponding to 30 k points in the irreducible Brillouin zone at which the Hamiltonian matrix was diagonalized. Upon convergence on energy ($\Delta E \sim 10^{-6}$ hartree), the periodic wavefunction based on the optimized geometry was obtained. The coordinates of H atoms were relaxed, but the unit cell was kept fixed. The index generation scheme proposed by Le Page & Gabe (1979) was applied to generate 15 074 unique Miller indices up to s = 1.2 Å^{-1} reciprocal resolution. The option XFAC of the *CRYSTAL09* program was then used to generate a set of static theoretical structure factors from the computed electron density.

All the electron-density refinements were performed with the *MoPro* program (Guillot *et al.*, 2001; Jelsch *et al.*, 2005) and the resulting dipole moments were calculated with *VMoPro* with the origin at the centre of mass and drawn in *MoProViewer* (Guillot, 2011).

2.2. Refinement *versus* theoretical structure factors – charge-density models

2.2.1. Multipolar Hansen–Coppens model (MM_{theo}). Multipolar refinement was performed using the Hansen–Coppens (Hansen & Coppens, 1978) model implemented in the *MoPro* package (Guillot *et al.*, 2001; Jelsch *et al.*, 2005). The pseudoatom electron density is described by

$$\rho_{\rm atom}(r) = \rho_{\rm core}(r) + P_{\rm val}\kappa^3\rho_{\rm val}(\kappa r) + \sum_l \kappa'^3 R_l(\kappa' r)\sum_m P_{lm\pm}(\theta,\varphi), \quad (1)$$

where the first two terms are the spherically averaged core and valence electron densities of the atom, and the last term corresponds to expansion/contraction of the non-spherical valence density in terms of real spherical harmonic functions. $P_{\rm val}$ is the valence population, $P_{lm\pm}$ are the multipole populations, and κ and κ' are the contraction/expansion parameters. R_l is a radial Slater-type function:

$$R_l(r) = \frac{\xi_l^{n_l+3}}{(n_l+2)!} r^{n_l}\exp(-\xi_l r), \quad n_l \geq l. \quad (2)$$

The O, C and N atoms were refined up to octupole or hexadecapole level ($l_{\rm max}$ = 3 or 4) and the H atoms up to dipole or quadrupole level ($l_{\rm max}$ = 1 or 2). The n_l and ξ_l values were equal to 2, 2, 2, 3, (4) and 4.466 au^{-1} (for O), 2, 2, 2, 3, (4) and 3.176 au^{-1} (C), 2, 2, 2, 3, (4) and 3.839 au^{-1} (N), and 1, 1, (2) and 2.000 au^{-1} (H). The n_l values in parentheses are for the hexadecapole and quadrupole level for non-H and H atoms, respectively. The core and valence scattering factors were calculated from Clementi & Roetti (1974) wavefunctions.

The least-squares refinement *versus* theoretical structure factors was performed using all reflections up to s = 1.2 Å^{-1}. The refinement strategy was as follows:

(i) The electroneutrality constraint was applied during the whole refinement process in all presented models.

(ii) The atomic displacement parameters (ADPs) were set to zero.

(iii) The atomic positions were not refined and H-atom distances were constrained to the standard neutron values (Allen *et al.*, 2006).

(iv) The multipolar and valence populations and contraction/expansion coefficients (P_{lm}, $P_{\rm val}$, κ, κ', $\kappa_{\rm core}$ for non-H atoms) were refined successively and then all together in the final refinement cycles.

Whatever the refinement strategy, a significant depletion of electron density at the non-H-atom positions occurred (Fig. S1 in the supplementary material[1]) due to the different wavefunctions used in *CRYSTAL09* (atomic Gaussian-type orbitals, DFT) and for the multipolar refinement (Clementi & Roetti–Slater-type expansion, Hartree–Fock). This was then modelled in two ways: (i) by refining a non-physical scale factor [average value K = 0.993 (1) for all tests]; and (ii) by refining a non-physical $\kappa_{\rm core}$ expansion/contraction coefficient for the core electron density of non-H atoms – one kappa per atom type [$\kappa_{\rm C}$ ~0.991 (2), $\kappa_{\rm N}$ ~0.992 (1) and $\kappa_{\rm O}$ ~0.994 (1), on average for all tests].

These small deviations of the scale factor or of $\kappa_{\rm core}$ parameters from unity significantly reduced the negative electron density from Fourier residual maps, as shown in Fig. S1. Rescaling the core scattering factor by introducing one $\kappa_{\rm core}$ per atom type was found to be superior, as already suggested by Pillet *et al.* (2001) in the test study on multipole refinement against theoretical corundum structure factors which accounted for the difference between DFT and Hartree–Fock (HF) core densities. Therefore Tables 1–3 present the results including a $\kappa_{\rm core}$ refinement, whereas Table S1 in the supplementary material gives the results with a scale-factor refinement.

Different orders of multipolar expansion were tested along with optimal restraints on symmetry and similarity of chemically equivalent atoms as recently determined in free-*R*-factor calculations (Paul, Kubicki, Kubas *et al.*, 2011); constraints on κ H atoms (default value 1.16; Stewart *et al.*, 1965) were also tested.

2.2.2. Virtual-atom model (VIR$_{\rm theo}$). The virtual-atom model (Dadda *et al.*, 2012) introduces a simplification in the multipolar model and was designed by us to be routinely used in macromolecular modelling. This approach describes the electron density as a superposition of real and virtual spherical atoms:

$$\rho(r) = \sum_{\rm atom}[\rho_{\rm atom}^{\rm core}(r) + P_{\rm atom}^{\rm val}\kappa^3\rho_{\rm atom}^{\rm val}(\kappa r)] + \sum_{\rm vir} P_{\rm vir}\kappa_{\rm vir}^3\rho_{\rm vir}(\kappa r), \quad (3)$$

where $\rho_{\rm core}$ and $\rho_{\rm val}$ are the core and spherical valence electron densities that can be calculated from HF or DFT methods. The real atoms (C, O, N, H) have a spherical symmetry and are described by the first and second terms of equation (3). The third term corresponds to the deformation electron density $\rho_{\rm vir}$ generated by the additional virtual atoms, which take asphericity into account. In this approach, the last term in equation (1) is eliminated, *i.e.* all multipolar populations are reduced to monopoles and additional virtual spherical atoms are initially placed on the positions of covalent bonding electron density and of electron lone pairs (with a starting monopole value $P_{\rm val}$ = 0).

A similar point-charge model has already been applied in a few cases in the literature: it was reported for urea (Scheringer, Kutoglu *et al.*, 1978; Scheringer, Mullen *et al.*, 1978; Mullen & Hellner, 1978*a*), thiourea (Scheringer, Kutoglu *et al.*, 1978; Scheringer, Mullen *et al.*, 1978; Mullen & Hellner, 1978*b*), diborane (Mullen & Hellner, 1977; Scheringer, Mullen & Hellner, 1978), decaborane (Dietrich *et al.*, 1979), cyanuric acid (Dietrich *et al.*, 1979) and silicon (Scheringer, 1980). More recently, a bond scatterers model was applied by Afonine *et al.* (2004, 2007) for ultra-high-resolution protein refinement.

There is an automatic procedure in the software *MoPro* (Jelsch *et al.*, 2005) which allows one to generate the coordinates of such virtual atoms as well as the restraints/constraints being applied on their geometries. The virtual atoms generated by *MoPro* are depicted in Fig. 2 as green spheres. The Q_{AB} and $Q_{\rm Lp}$ virtual atoms refer, in this paper, to the bonding density between atoms A and B, and to the charge located on the expected oxygen lone-pairs site, respectively.

In this approximation, all atoms (real and virtual ones) have spherical symmetry. Refinement against the theoretical data concerns therefore only spherical κ coefficients and $P_{\rm val}$

[1] Supplementary material for this paper has been deposited in the IUCr electronic archives (Reference: PC5017). Services for accessing these data are described at the back of the journal.

valence populations of all atoms (using an electroneutrality constraint), and the coordinates of virtual atoms.

Up to now, only one type of virtual atom is available, the electron density of which, $\rho_{vir}(r)$, was fitted using Slater functions from a Fourier residual density computed using theoretical structure factors and after a spherical atoms (independent-atom model) refinement. For this purpose, a centrosymmetric crystal of DL-histidine (Coppens *et al.*, 1999) was selected and the theoretical structure factors were computed from *ab initio* calculations. The residual density was fitted in a [0., 1] Å interval around the Cα—Cβ bonding electron-density peak of the amino acid in the plane perpendicular to the Cα—Cβ bond to avoid effects of the neighbouring C atoms. The Slater function coefficients and $\rho_{vir}(r)$ curve are shown in Dadda *et al.* (2012).

Models with different levels of restraints on the charge density (*e.g.* chemical similarity) imposed only on the virtual atoms or also on real atoms were tested. The default stereochemical restraints include linearity (the virtual-atom position is restrained to stay on the line connecting two bonded atoms), distances, planarity and similarity of angles.

Soft linearity restraints (σ = 0.1 Å) were applied because of a lack of convergence in calculations using stronger restraints. The lone-pairs (N—O—Lp $\simeq$ N—O—Lp′) angle similarity restraint was removed for the NO_2 group to take into account the high peaks of positive electron density in the Fourier residual maps on both sides of each O atom. An additional virtual atom was introduced on the N=O bonds, close to the O atom (Fig. 2), to reduce the high negative residual density peak located on the bond. To compare the results with and without these additional atoms, see Table S4 in the supplementary material.

To reduce the number of least-squares variables of the refinement, geometrical and chemical equivalences were applied to the corresponding virtual and real atoms (see footnotes to Table 3).

2.2.3. Kappa model (KM$_{theo}$). In the kappa model proposed by Becker and Coppens (Coppens *et al.*, 1979), the total electron density of an atom is defined by

$$\rho_{atom}(r) = \rho_{core}(r) + P_{val}\kappa^3\rho_{val}(\kappa r), \qquad (4)$$

where P_{val} is the valence population and κ is the spherical expansion/contraction coefficient. This model is simpler than the multipolar and the virtual-atom models, as the charges are attributed only to the real atoms and no aspherical deformation electron density is considered.

Coppens *et al.* (1979) were able to obtain reasonable values of the atomic charges and dipole moments for organic and inorganic compounds using this approximation for experimental and theoretical data, when comparing them with more sophisticated methods.

2.3. Refinements based on experimental data

The experimental details of the single-crystal diffraction may be found in Paul, Kubicki, Kubas *et al.* (2011). Refinements based on the experimental data were performed using the same three electron-density models (MM, VIR and KM) as for the theoretical data; however additional parameters, such as ADPs and coordinates, were refined knowing that the lack of special precautions (especially in the case of H atoms) can lead to wrong conclusions. The residual maps did not show any evidence that could suggest refining of any κ_{core} parameters for experimental data.

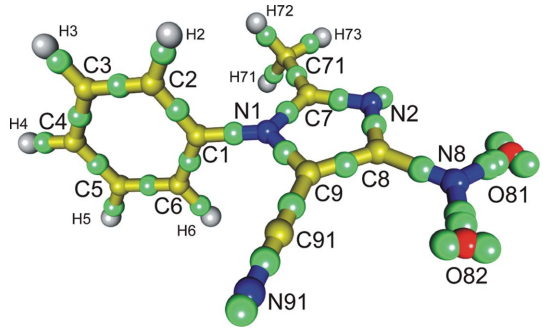

Figure 2
View of the molecule with the real-atom labelling and virtual atoms generated by *MoPro* depicted as green spheres (figure prepared with *MoProViewer*; Guillot, 2011). The model for the theoretical charge density has two virtual atoms on the N—O bond (one with $P_{vir} > 0$ and one with $P_{vir} < 0$).

2.3.1. Multipolar model (MM$_{exp}$). R_{free} restraints as defined in Paul, Kubicki, Kubas *et al.* (2011) were kept constant and various multipolar expansion levels for H and non-H atoms were tested. In models 4*c* and 4*f*, according to the theoretical fit (see below), hexadecapoles were refined for the cyano-group atoms (C91 and N91) as the bond charge concentration is quite significant, while the other non-H atoms were kept at the octupolar level.

As more parameters were refined compared to the theoretical models (*xyz* and U_{ij}), only restrained refinements were tested to avoid possible charge-density parameter correlations, which could influence the electrostatic properties. Details of the restraints used are given in the supplementary material. The high/low-order refinements were performed to obtain reliable parameters for the H atoms as no neutron data were available. High-order refinements were performed for *xyz* and U_{ij} of non-H atoms followed by low-order refinement of positions and isotropic displacement parameters of H atoms, and then H-atom positions were moved to neutron distances. Then the ADPs of H atoms were estimated using the *SHADE2.1* server (Madsen, 2006), and their κ and κ' parameters were, respectively, restrained to 1.16 and 1.25 (σ_r = 0.01), which were found to be the best values after the theoretical structure-factor refinement. The H-atom positions and ADPs were refined in the last cycle [with constrained neutron distances and restraints on the ADPs, $U_{ij} \simeq U_{ij}$ (*SHADE*) with σ = 0.005 for U_{11}, U_{22}, U_{33} and σ = 0.0005 for U_{12}, U_{23}, U_{13}] to avoid their correlations with κ and P_{val}, as some difficulties were already observed for the theoretical data refinement. For comparison, the results for models using H-atom ADPs constrained to *SHADE* are also presented. It will be shown that the H-atom treatment, *i.e.* the choice of κ and refinement of ADPs, as well as the choice of the order of

multipolar expansion, has a great influence on the dipole moment.

2.3.2. Virtual-atom model (VIR_{exp}). In the VIR_{exp} model (Dadda *et al.*, 2012), the calculations were performed based on the geometry obtained after high/low-order refinement of experimental data. The H atoms were moved to the neutron positions and refined with these H—*X* distances constrained in the final cycles, *i.e.* the H—*X* direction was refined at constant bond length. The ADPs of H atoms were obtained from *SHADE* and either refined with the same restraints as above for MM_{exp} just before the final cycles of refinement for models 5*a*–5*d*, or kept constrained. For models 5*e*–5*h* the σ of restrained H-atom ADPs was reduced by a factor of 5, due to unrealistic ellipsoids obtained with initial values. ADPs of the bond virtual atoms were constrained to the average values of the two neighbours. For the lone pairs, the ADPs were constrained to ride on the refined value of the carrying atom. At first, valence populations and κ of all atoms were refined, followed by the virtual-atom positions. Then the refinement of ADPs and *xyz* of all real non-H atoms was performed. The additional negative virtual atoms on the N=O bonds were implemented, even if not deemed necessary. The density was already well described with one virtual atom on this bond, but the comparison with the theoretical results would not be consistent.

2.3.3. Kappa model (KM_{exp}). The kappa model is obtained by setting the multipoles of atoms to zero. The final geometry from the multipolar refinement is kept, with no further refinement of coordinates and thermal motions, while the P_{val} parameters of all atoms and κ of non-H atoms are refined until convergence.

Besides the multipolar geometry, the virtual geometry was also tested. This second geometry is the same as in VIR_{exp}, *i.e.* geometry after high/low-order refinement, with H atoms moved to the neutron H—*X* distances and with their ADPs generated by *SHADE*.

It appeared that any attempts to refine the geometry obtained after high/low-order refinement (virtual geometry), including *xyz* and ADPs or not, resulted in dipole-moment magnitudes close to the theoretical ones, but the directions were always incorrect. In contrast, for the multipolar geometry, the directions were close to the multipolar dipole moment. Therefore the multipolar geometry was chosen for further kappa-refinement tests.

2.4. Dipole-moment calculations

The molecular dipole moments $\boldsymbol{\mu}$ are calculated with the origin at the centre of mass, based on atomic net charges and atomic dipoles, according to the formula

$$\boldsymbol{\mu}_{\text{total}} = \sum_i \boldsymbol{\mu}_i + \sum \mathbf{r}_i q_i. \quad (5)$$

Owing to the electroneutrality constraint, $\boldsymbol{\mu}$ is actually independent of the origin. The atomic dipole-moment contributions are dependent on eight variables: the net charge derived from P_{val}, the κ parameter, the coordinates and the three dipole populations P_{10}, P_{11+} and P_{11-}. Only dipolar terms in the multipole expansion contribute to the dipole moment (Coppens, 1997).

3. Results

The dipole-moment magnitudes obtained with DFT methods at the B3LYP/6-31G(d,p) level of theory are 9.17 D for a single molecule and 10.61 D for the periodic system using a Bader AIM partitioning (Bader, 1990); this latter value can be taken as a reference to rank the calculations based on theoretical structure factors. This reference is not strictly valid for the experimental data because no experimental dipole measurement is available.

As the coordinates and ADPs were not refined against theoretical data, the correlations between the refined parameters, that have an impact on the total dipole moment, are small compared to experimental data.

3.1. Multipolar refinements against theoretical structure factors (MM_{theo})

Of the numerous refinements performed, 12 are reported in Table 1 (models 1*a*–1*l*). The varied parameters are: (*a*) order of multipolar expansion of H and non-H atoms; (*b*) κ_{hyd} refined or constrained to 1.16; (*c*) R_{free} restraints applied or not on the symmetry and similarity of the charge distribution of equivalent atoms.

As expected, the crystallographic agreement factors are better for models with more parameters refined. The goodness of fit at the convergence should be close to zero for theoretical data (unit weighting schemes) rather than unity for the experimental refinements (Moss *et al.*, 1995). The quality of refinements is confirmed by the Fourier residual and static electron-density maps (Fig. S2); the largest residual electron densities (0.20–0.25 e Å^{-3}) are related to the high resolution used for calculations (s = 1.2 Å^{-1}). With an $s \leq 1.0$ Å^{-1} resolution cutoff, all these residual electron-density values drop by ∼0.1 e Å^{-3} for models 1*a*–1*h* and by 0.05 e Å^{-3} for models 1*i*–1*l*, for both positive and negative peaks. This residual electron density is spread over the molecule in the regions of heteroatomic bonds. It is important to note that the multipolar model works much better when describing the bonding electron density between atoms of the same type (C—C bonds, for example). This is related to the radial expansion parameters (Moss *et al.*, 1995).

As shown in Table 1, the dipole-moment magnitudes range between 13.3 D (refinement 1*f*) and 10.1 D (refinement 1*i*) compared to the expected 10.6 D theoretical value. The direction of the moment can be described by the difference between the vector calculated in *CRYSTAL09* and the $\boldsymbol{\mu}$ vector from the appropriate refinement. The difference angle varies from 12.6° (1*a*) to 14.7° (1*l*). This angular dispersion is small, as also shown in Fig. 3, and the systematic angular difference is surprising; it may be related to the partitioning used for the theoretical dipole-moment calculation in the solid state (AIM method). The MM_{theo} dipole moments are larger than the theoretical one (10.6 D) for models using hexadeca-

Table 1
MM_{theo} refinements (kappa core refined).

N_{obs} = 15 074 to s = 1.2 Å^{-1}. Dipole-moment modules [dipole generated by the atomic monopoles (P_{val})] and the atomic dipoles are given in parentheses. HEX – hexadecapole, OCT – octupole, QUA – quadrupole, DIP – dipole, R_{free} restraints – restraints obtained *via* R_{free} calculations (Paul, Kubicki, Kubas *et al.*, 2011). Goof is the goodness of fit. Numbers in italics show the $\boldsymbol{\mu}$ values obtained from refinements under special conditions, different to those considered as standard.

Model	Multipolar order non-H/H	κ_{hyd}	No. of variables	Restraints applied	*RF*, *wR2F* (%)	Goof	$\boldsymbol{\mu}$ total (monopoles/dipoles) (D)	$\boldsymbol{\mu}$ total (monopoles/dipoles) (D) only for significant HEX/QUA	Angle between $\boldsymbol{\mu}_{theo}$ and $\boldsymbol{\mu}_{calc}$ vectors
1*a*	HEX/QUA	refined	534		0.421 0.423	0.051	12.11 (11.26/2.48)	*11.64 (10.80/2.60)*	12.6
1*b*	HEX/QUA	1.16	534		0.424 0.426	0.052	13.02 (12.22/2.37)	*12.95 (12.17/2.40)*	12.9
1*c*	OCT/DIP	refined	341		0.505 0.547	0.066	10.71 (10.90/1.57)		13.0
1*d*	OCT/DIP	1.16	341		0.513 0.568	0.068	11.11 (10.76/1.43)	13.7	
1*e*	HEX/QUA	refined	534	R_{free}	0.433 0.442	0.027	12.42 (11.12/2.50)	*11.98 (10.67/2.52)*	14.0
1*f*	HEX/QUA	1.16	534	R_{free}	0.435 0.445	0.040	13.28 (12.02/2.43)	*13.21 (11.96/2.38)*	14.5
1*g*	OCT/DIP	refined	341	R_{free}	0.514 0.564	0.063	11.00 (10.56/1.34)		14.2
1*h*	OCT/DIP	1.16	341	R_{free}	0.521 0.585	0.059	11.33 (10.44/1.48)		14.3
1*i*	OCT and HEX (C≡N)/DIP	refined	359		0.501 0.537	0.065	10.14 (10.32/2.34)		13.2
1*j*	OCT and HEX (C≡N)/DIP	1.16	359		0.509 0.559	0.067	10.58 (10.27/2.26)		14.0
1*k*	OCT and HEX (C≡N)/DIP	refined	359	R_{free}	0.509 0.555	0.060	10.32 (9.91/2.14)		14.5
1*l*	OCT and HEX (C≡N)/DIP	1.16	359	R_{free}	0.518 0.577	0.057	10.87 (9.96/2.22)		14.7

polar functions for all non-H atoms and quadrupoles for H atoms. Compared to theory, the closest values of the dipole-moment magnitudes are obtained for models 1*i*–1*l*, with octupole/dipole non-H/H-atom treatment and with hexadecapolar description of the very electron-rich cyano atoms, whatever the type of restraints.

The directions of selected total dipole moments and their components (contributions from atomic dipoles and monopole charges) are depicted in Fig. 3 (all models are deposited as Figs. S3–S4). The contribution from the atomic dipoles is constantly larger in models with higher multipolar expansion (see also Table 1) but the maximal difference (1*e*–1*g*) is only 1.16 D. For the $\boldsymbol{\mu}$ derived from the monopole charges, the maximal difference is 2.31 D (1*b*–1*k*). It results in a maximum difference for the total $\boldsymbol{\mu}$ of 3.14 D between models 1*f* and 1*c*, *i.e.* more than 25%.

In general, the following factors increase the dipole-moment modulus:

(*a*) Multipole expansion: a higher order of multipolar expansion of H atoms (quadrupolar) and non-H atoms (hexadecapolar) leads to higher $\boldsymbol{\mu}$. This is also noticed for the experimental data, where models with OCT_{nonH}/QUA_{HYD} are analysed. Nevertheless, most quadrupolar terms of hydrogen expansion are not statistically significant (at the 5σ level), except the $2z^2 - (x^2 + y^2)$ quadrupole along the H—*X* axis. In fact, refinement with only significant quadrupoles (HYD) and hexadecapoles (NOH) lowers the $\boldsymbol{\mu}$ values in models 1*a*, 1*b*, 1*e* and 1*f* by 3.9, 0.54, 3.5 and 0.60%, respectively, with no changes in *R*-factor statistics. The great impact of the H atoms may be due to their location at the opposite side of the molecule with respect to the electronegative nitro and cyano groups.

(*b*) κ_{hyd} refinement: the models with refined κ_{hyd} give slightly higher values of dipole moments (average +1.0% of

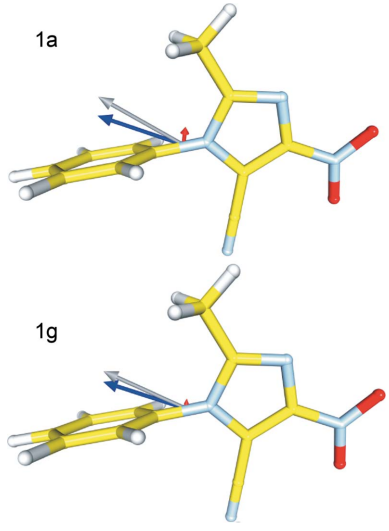

Figure 3
Dipole-moment directions (grey, total; red, contribution from atomic dipoles; blue, contribution from atomic charges) for selected models 1*a* and 1*g*.

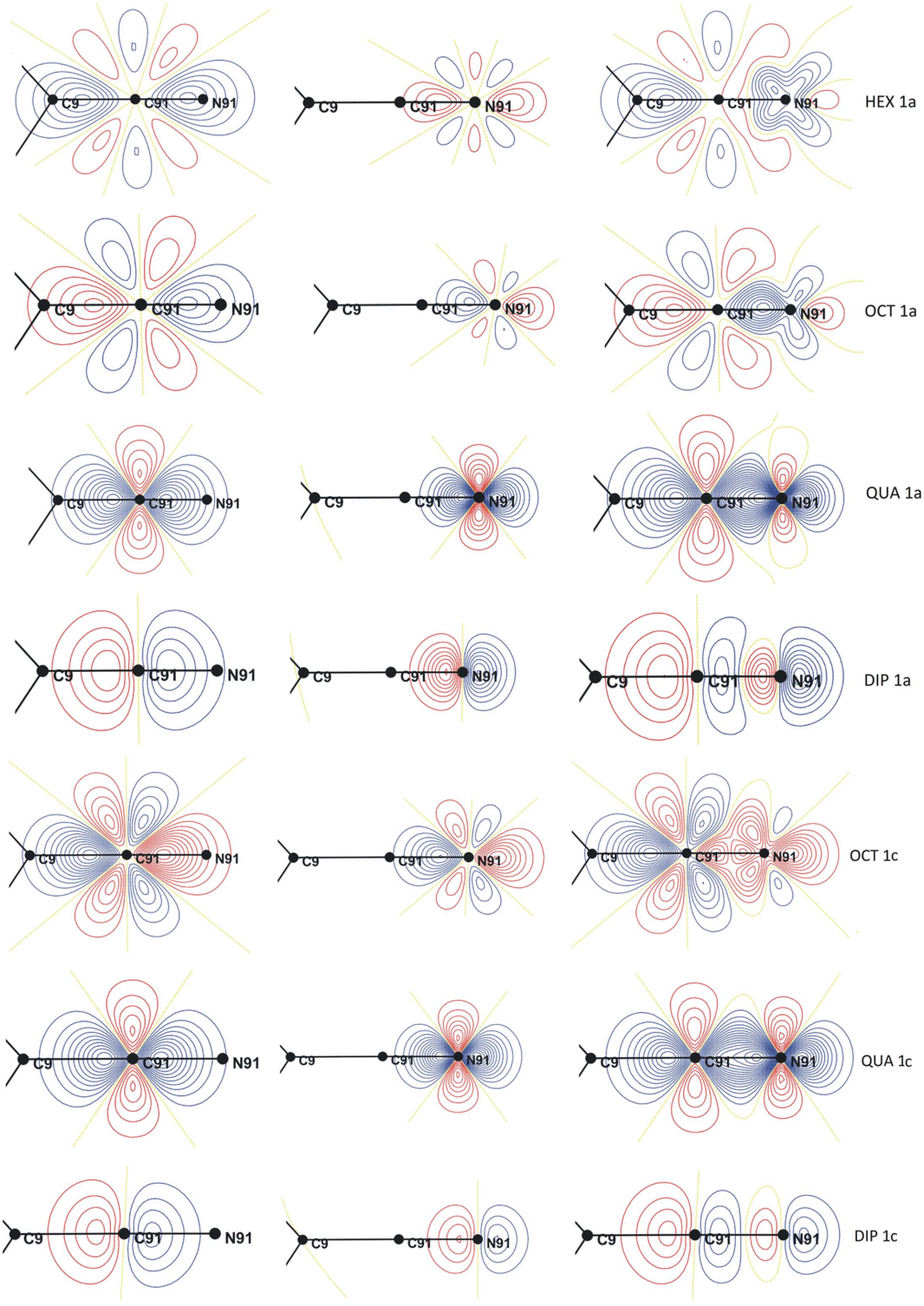

Figure 4
Multipolar electron density for atom C91 (left), N91 (middle) and the complete C≡N group (right). The contribution of the different multipole levels is shown. Model 1*a*, lines 1–4: HEX, OCT, QUA and DIP. Model 1*c*, lines 5–7: OCT, QUA and DIP. Contour levels are ±0.05 e Å^{-3} for the DIP and QUA, and ±0.005 e Å^{-3} for the OCT and HEX contributions.

difference) compared to those with κ_{hyd} fixed to 1.16. Nevertheless all these differences are within 3σ.

(*c*) R_{free} restraints: the application of soft R_{free} restraints for the current charge-density analysis does not influence significantly the P_{val} values, compared to the unrestrained refinement.

As expected, the lowest H-atom valence populations are connected with the highest corresponding κ_{hyd}. The average P_{val_hyd} in both 1*c* and 1*g* is 0.86 e (κ = 1.19), while in 1*a* and 1*e* it is 0.93 e (κ = 1.15). In models with constrained κ_{hyd}, P_{val} has intermediate values. For non-H atoms, the largest differences are found for the C≡N atoms [P_{val} (C91) = 4.53 (1) (1*a*, 1*b*, 1*e*,

Table 2
Topological characteristics of the bond critical points for the C≡N group in models 1*a* and 1*c*.

D_{12} – distance between the two atoms, $D_{1,2cp}$ – distance from atom 1 or 2 to critical point (cp), ρ_{tot} – total electron density at cp, $\nabla^2\rho$ – Laplacian at cp, $\lambda_{1,2,3}$ – Hessian eigenvalues, ε – ellipticity at cp.

cp	Atom 1	Atom 2	D_{12} (Å)	D_{1cp} (Å)	D_{2cp} (Å)	ρ_{tot} (e Å^{-3})	$\nabla^2\rho$ (e Å^{-5})	λ_1 (e Å^{-5})	λ_2 (e Å^{-5})	λ_3 (e Å^{-5})	ε
Model 1*a*											
cp1	C9	C91	1.4110	0.6798	0.7314	1.94	−15.6	−13.4	−12.2	10.0	0.09
cp2	C91	N91	1.1580	0.4029	0.7551	3.23	−13.5	−25.7	−25.4	37.6	0.01
Model 1*c*											
cp1	C9	C91	1.4110	0.6890	0.7220	1.91	−14.0	−13.2	−11.5	10.7	0.13
cp2	C91	N91	1.1580	0.4070	0.7510	3.22	−14.1	−24.9	−24.9	35.7	0.00

1*f*) and 4.35 (1) e (1*c*, 1*d*, 1*g*, 1*h*), P_{val} (N91) = 4.68 (1) (1*a*, 1*b*, 1*e*, 1*f*) and 4.82 (1) e (1*c*, 1*d*, 1*g*, 1*h*)], and for the methyl carbon atom, which is influenced by the valence population changes of its H atoms. The low H71, H72 and H73 P_{val} values in 1*c* and 1*g* are in line with a higher C71 P_{val}.

(*d*) Atomic dipole contributions: for the H atoms, the only significant dipole is P_{10}, along the C—H bond direction. The lowest atomic $\boldsymbol{\mu}_{dip}$ (atomic dipole contributions only) occur in 1*c* and 1*g* (H dipole expansion with κ_{hyd} refined), whereas the highest $\boldsymbol{\mu}_{dip}$ is obtained with H quadrupolar expansion.

For non-H atoms, the highest $\boldsymbol{\mu}_{dip}$ are found on the two electronegative groups (C≡N and NO_2). The C91 and N91 dipoles are significant along the triple bond, according to their cylindrical symmetry. The C91 $P_{1,0}$ value is ∼0.385 (2) in the HEX/QUA model and 0.310 (6) in OCT/DIP. For N91, $P_{1,0}$ ∼−0.133 (1) in the HEX/QUA model and −0.119 (1) in the OCT/DIP. The most significant atomic dipoles in the nitro group are the following: P_{11+} [N8: −0.027 (3), O81 = O82: −0.116 (1) for HEX/QUA; and N8: −0.021 (3), O81 = O82: −0.115 (2) for OCT/DIP].

Fig. 4 compares all C≡N atomic multipolar contributions for models 1*a* and 1*c*, for which the discrepancies between the C≡N atoms' valence populations are the highest. Whereas the quadrupolar terms are statistically equal, the dipolar contributions change considerably when hexadecapoles are added. Fig. 5 gives the static deformation and Laplacian maps of the C≡N group for both 1*a* and 1*c* refinements and Table 2 lists the associated topological properties. All the electron-density features are similar within the standard deviation. Therefore, augmenting the order of the multipole extension greatly affects the dipole contribution to the dipole moment without changing the electron-density topology. Over-parametrization must therefore be avoided, especially for such a calculation.

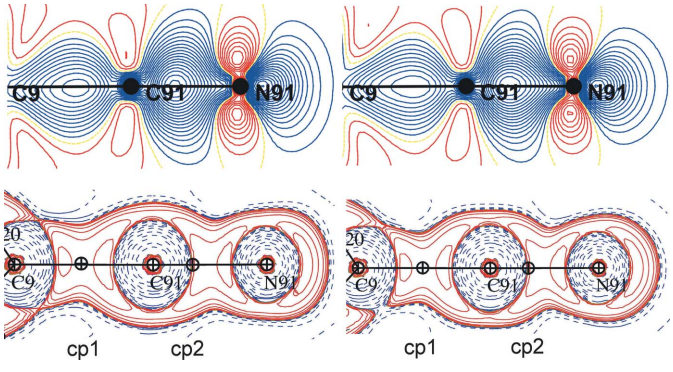

Figure 5
Static deformation electron density and Laplacian maps for C≡N groups of models 1*a* (left) and 1*c* (right); contour ±0.05 e Å^{-3} (static deformation) and 100 e Å^{-5}; blue positive, red negative; cp1, bond critical point on C9—C91; cp2, bond critical point on C91≡N91.

In conclusion, the hexadecapolar expansion of atoms not belonging to the cylindrical C≡N group is unnecessary for a thorough estimation of the dipole moment from theoretical structure-factor refinement. The same applies to the quadrupolar expansion for H atoms (see the results of refinement with only significant HEX/QUA populations – last column in Table 1).

Finally, when the scale factor is refined instead of κ_{core}, an increase in the dipole moment of 2.5 D is observed, almost exclusively due to a higher contribution of the atomic charges (see Table 1 and Table S1 in the supplementary material). On average the $\boldsymbol{\mu}_{monopole}/\boldsymbol{\mu}_{dipole}$ ratio is 7.6 for models where the scale factor is refined (models 1*m*–1*t*) and 5.5 for models with κ_{core} refined (see Table 1 and Table S1 in the supplementary material).

The crystallographic statistics, dipole-moment vectors and values of all discussed parameters are given in Table S2 in the supplementary material.

Some attempts were also made to refine the multipolar model only to a dipolar expansion for all atoms, but the refinements were not stable, due to κ' fluctuation of strongly electronegative groups, and no convergence was achieved.

3.2. Virtual-atom theoretical model (VIR$_{theo}$)

Two additional positive virtual atoms had to be introduced on the N═O bonds in the nitro group (Fig. 2), as a single virtual atom did not describe all the theoretical deformation density in this region. This addition modelled the negative N═O electron-density peak of 0.32 e Å^{-3} (Fig. 6).

Nine different virtual-atom models were tested with the following variables: κ_{hyd} (1.10, 1.13 and 1.16) and chemical equivalence restraints or constraints (Table 3). All nine models describe quite well the electron-density distribution (Fig. 6) – the static deformation maps are in good agreement with those obtained from MM$_{theo}$. However, the crystallographic agreement factors are systematically doubled

compared to MM_{theo}, as shown also by the residual maps (Fig. 6), a result in agreement with Dadda *et al.* (2012).

Restriction of κ_{hyd} was found to be crucial in limiting the influence of peripheral H atoms in the dipole-moment magnitude (models 2*j*–2*l* in Table S3). Freely refined κ_{hyd} values range between 1.19 and 1.26, leading to a too large dipole moment $17.3 < \boldsymbol{\mu} < 18.7$ D.

As shown in Table 3, the dipole-moment magnitude dispersion is small compared to MM_{theo}. The magnitude of $\boldsymbol{\mu}$ is in particularly good agreement with that computed directly from theory for $\kappa_{hyd} = 1.13$ and it is not influenced by the charge-density similarity restraints or constraints. Hence, parallel trends are observed among models 2*a*–2*c*, 2*d*–2*f* and

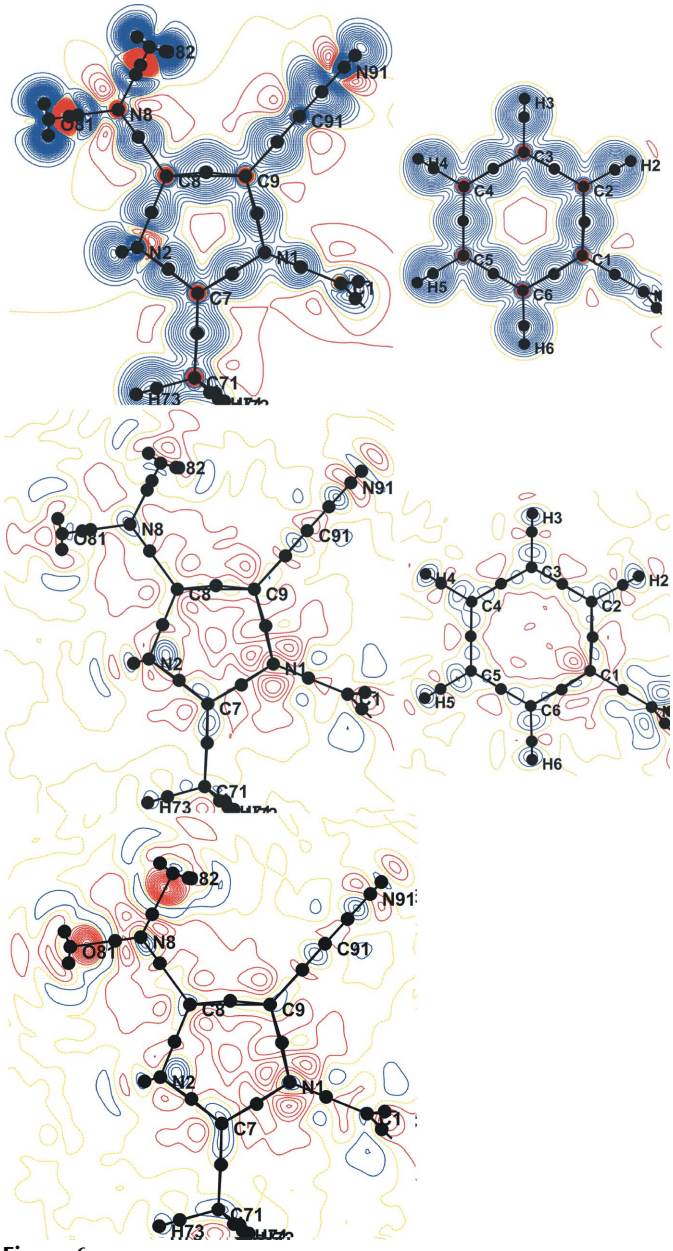

Figure 6
Static deformation and Fourier residual maps (reciprocal resolution up to $s = 1.0$ Å^{-1}) for model 2*b*; contour ±0.05 e A^{-3}. The last Fourier map was computed for the model without the additional virtual atoms on the N═O bonds.

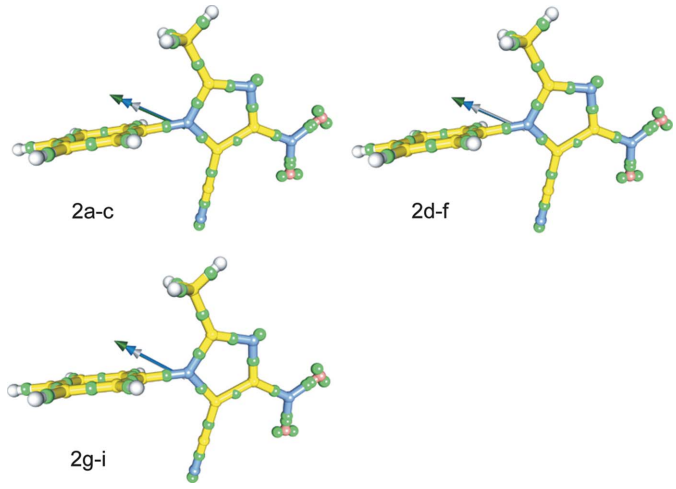

Figure 7
Dipole-moment directions in model 2. Grey: *a*, *d*, *g*; blue: *b*, *e*, *h*; green: *c*, *d*, *i*.

2*g*–2*i*: when κ_{hyd} increased by 0.03, $\boldsymbol{\mu}$ increases on average by 1.4 D (Fig. 7). Increasing κ_{hyd} is also directly related to H-atom valence populations, but the non-H κ coefficients remain rather stable (variation <1%) as for the virtual atoms (in general +2 to +3% except for the two negative virtual atoms on the N═O bonds: +6%). The maximal increase of non-H-atom valence population, 6%, is observed for the C71 methyl atom. For the other atoms, P_{val} increases from 2 to 3% with $\kappa_{hyd} = 1.16$ compared to $\kappa_{hyd} = 1.10$. There is no clear tendency for the virtual-atom valence populations. The P_{val} changes between corresponding models 2*a* and 2*c*, 2*d* and 2*f*, and 2*g* and 2*i* can be +6% (C71) for real and +12% for the virtual atoms, but reach 50% (difference of 0.15 e) for those on the N═O bonds.

The dispersion of the differential angle between the theoretical one from *CRYSTAL09* and from virtual-atom modelling is very small (from 14.6 to 15.4°, Table 3) and does not stand out from the MM_{theo} results.

It is noteworthy that, in this modelling, all real atoms bear positive charges and all but two virtual atoms have a negative charge ($P_{vir} > 0$). This virtual-atom modelling seems very appropriate to extract dipole moments from theoretical structure factors. This can be easily understood because this model partitions the space with dipoles (+ on the atoms, − on the bonds). The optimal value of H-atom κ is 1.13 to obtain the best moment, but one should keep in mind that the doubling of virtual atoms on the nitro N═O bonds is essential to achieve featureless residual maps, and simultaneously this causes a significant decrease of the molecular dipole moment.

3.3. Kappa model (KM_{theo})

Six different models were tested for the KM_{theo} modelling, with the following variable conditions (Table 4): (*a*) κ_{hyd} constrained to 1.4, as suggested by Coppens (1997); or (*b*) κ_{hyd} freely refined with 1.4 as a starting value; (*c*) different levels of equivalent-atom similarity restraints.

Table 3
Dipole moments from the virtual-atom refinements against theoretical structure-factor moduli.

Restraints on virtual atoms: linearity $\sigma_l = 0.1$ Å; distances: $d(H-Q) = 0.37$ Å with $\sigma_d = 0.01$ Å, Lp $d(O, Lp) = 0.28$ Å with $\sigma_d = 0.01$ Å; distance similarities: $d(O, Lp)$ $\sigma_d = 0.01$ Å; planarity (Lp) $\sigma_p = 0.001$.

Model	Restraints/constraints	No. of variables	*RF*, *wR2F* (%)	Goof	Dipole moment (D)	Angle between $\boldsymbol{\mu}_{theo}$ and $\boldsymbol{\mu}_{calc}$ vectors
2*a*	$\kappa_{hyd} = 1.1$	215	0.775 0.941	0.112	9.23	14.6
2*b*	$\kappa_{hyd} = 1.13$	215	0.764 0.927	0.111	10.74	14.7
2*c*	$\kappa_{hyd} = 1.16$	215	0.756 0.918	0.110	12.27	14.9
2*d*	$\kappa_{hyd} = 1.1$ chem. equiv. rest.†	215	0.774 0.941	0.112	9.28	15.2
2*e*	$\kappa_{hyd} = 1.13$ chem. equiv. rest.†	215	0.763 0.926	0.111	10.48	15.4
2*f*	$\kappa_{hyd} = 1.16$ chem. equiv. rest.†	215	0.756 0.917	0.109	11.97	15.4
2*g*	$\kappa_{hyd} = 1.1$ chem. equiv. cons.‡	205	0.770 0.939	0.112	9.36	15.1
2*h*	$\kappa_{hyd} = 1.13$ chem. equiv. cons.‡	205	0.767 0.928	0.111	10.42	15.2
2*i*	$\kappa_{hyd} = 1.16$ chem. equiv. cons.‡	205	0.759 0.918	0.110	11.90	15.3

† Chemical equivalence restraints on non-virtual atoms, with $\sigma = 0.01$ (κ and valence populations of): C2 ≃ C6; C3 ≃ C5; O81 ≃ O82; H2 ≃ H6; H5 ≃ H3; H71 ≃ H72 ≃ H73. ‡ Constrained atoms the same as in † but with $\sigma = 0.0$.

Table 4
Results of the KM_{theo} refinements.

No. of reflections = 15 074.

Model	Restraints/ constraints	No. of variables	κ_{hyd}	*RF*, *wR2F* (%)	Goof	Dipole moment (D)	Angle between $\boldsymbol{\mu}_{theo}$ and $\boldsymbol{\mu}_{calc}$ vectors
3*a*	constraints†	38	1.4	1.950 2.763	0.329	11.25	13.8
3*b*	restraints†	45	1.4	1.953 2.764	0.329	11.28	13.5
3*c*		45	1.4	1.954 2.766	0.329	11.38	14.0
3*d*	constraints	42	refined	1.914 2.748	0.327	8.78	16.0
3*e*	restraints	53	refined	1.912 2.747	0.327	8.55	15.5
3*f*		53	refined	1.910 2.747	0.327	8.06	15.6

† Definition of chemical equivalency of atoms is the same as in VIR_{theo} (see footnotes to Table 3).

The crystallographic agreement factors are much higher than in the two previous models because of the aspherical electron density which is not incorporated.

The dipole-moment magnitudes obtained are slightly higher than in the theoretical calculations for models with a constrained κ_{hyd} value and drop when kappa is refined. The $\boldsymbol{\mu}$ directions compared with the theoretical one are also closer for κ_{hyd}-constrained models (Table 4 and Fig. 8).

Restrictions imposed on κ_{hyd} are crucial as they significantly influence the dipole-moment magnitudes, while the chemical-equivalence similarity constraints/restraints have almost no effect.

All κ and P_{val} values are collected in Table S5 in the supplementary material.

3.4. Conclusion – theoretical structure factors

Compared to a reference value of 10.6 D taken from a *CRYSTAL09* computation, we were able to obtain a very good agreement in the modulus and direction of the dipole moment for the two MM and VIR models. The differential angle between the theoretical $\boldsymbol{\mu}$ vector and vectors obtained in the calculations lies between 12.9 and 16.0°. Each group of sub-models requires specific constraints imposed on the κ of H atoms. The constraints/restraints on the symmetry and chemical equivalency play a minor role. In addition, in the multipolar atom model, the choice of the order of multipolar expansion is a key issue. Over-parametrization must be avoided.

3.5. Experimental data refinements

3.5.1. Multipolar model (MM_{exp}). According to the theoretical calculations, to obtain a reliable $\boldsymbol{\mu}$ value, the order of multipolar expansion should be fixed at a dipolar level for H atoms, an octupolar level for non-H atoms and hexadecapoles must be used for electron-rich bonds with cylindrical symmetry like C≡N. Together with the level of multipolar expansion, the treatment of ADPs of H atoms obtained from *SHADE* (constrained or restrained) was tested. The optimal restraints on symmetry and similarity on chemically equivalent atoms were kept in all refinements (for details see §2).

The summary for the MM_{exp} calculations is presented in Table 5.

Table 5
Results of the MM_{exp} refinement.

$I/\sigma(I) > 2$, $s_{max} = 1$ Å^{-1}; 6164 reflections. The total dipole-moment magnitudes are shown first, parts derived from monopoles and atomic dipoles are in parentheses. HEX – hexadecapole, OCT – octupole, QUA – quadrupole, DIP – dipole.

Model	Multipolar level non-H/H atoms	No. of variables	*RF*, *wR2F* (%)	Goof	Total $\boldsymbol{\mu}$ (monopoles/dipoles) (D)	$\boldsymbol{\mu}$ total (monopoles/dipoles) (D) only for significant HEX/QUA	$\boldsymbol{\mu}$ total (monopoles/dipoles) (D) with H-atom ADPs constrained to *SHADE* values	Angle between $\boldsymbol{\mu}_{theo}$ and $\boldsymbol{\mu}_{calc}$ vectors
4*a*	HEX/QUA	757	2.32 2.27	0.771	10.91 (12.91/2.65)	*11.21 (12.95/2.76)*	*11.87 (14.62/3.21)*	33.6†/35.4‡
4*b*	OCT/DIP	564	2.43 2.38	0.897	12.63 (13.50/0.96)		*11.74 (13.42/1.73)*	15.4/18.4
4*c*	OCT and HEX (C≡N)/DIP	582	2.42 2.37	0.876	12.38 (13.15/1.64)		*11.14 (12.82/2.10)*	16.3/19.3
4*d*	HEX/DIP	717	2.36 2.31	0.784	9.44 (10.00/3.33)	*9.48 (10.07/3.33)*	*8.95 (10.25/3.55)*	11.8/12.2
4*e*	OCT/QUA	603	2.44 2.40	0.905	14.88 (16.15/1.50)	*14.47 (15.73/1.53)*	*14.25 (16.31/2.19)*	29.4/29.8
4*f*	OCT and HEX (C≡N)/QUA	622	2.430 2.384	0.883	14.12 (15.63/1.71)	*13.91 (15.41/1.64)*	*13.84 (16.15/2.41)*	29.9/30.6

† *SHADE* restraints. ‡ *SHADE* constraints.

For all refinements, the residual Fourier electron density is spread over the unit cell with insignificant concentrations or depletions in the middle of the phenyl ring and close to the triple bond of the C≡N group. As also seen by the crystallographic residual factors ($2.3 < wR2F < 2.4\%$), these maps do not allow one to select the best refinement.

The analysis of the dipole-moment magnitudes and directions (Fig. 9) leads to the following conclusions:

(*a*) If we refer to the theoretical calculation, which means we trust the theoretical value and direction, the best dipole-moment vectors are obtained for models 4*b*–4*c*, with dipolar expansion of H atoms and ADPs constrained to *SHADE* values, no matter what the expansion of C≡N is; the corresponding magnitudes are 11.7 and 11.1, respectively, close to the theoretical calculation.

(*b*) *SHADE* constraints imposed on the H-atom ADPs decrease the $\boldsymbol{\mu}$ values for all models but 4*a*, with the largest drop observed for model 4*c*, which is the multipolar expansion predicted from theoretical calculations, to generate the $\boldsymbol{\mu}$ value closest to the theoretical one (see above); in addition the *SHADE* ADP constraints increase the difference between the angles of the calculated and theoretical $\boldsymbol{\mu}$ vectors.

(*c*) For the models with H-atom ADPs constrained, $\boldsymbol{\mu}_{dip}$, computed from the atomic dipole contribution only, is systematically larger than when H-atom ADPs are restrained.

(*d*) Refinement of significant hexadecapoles and quadrupoles in models 4*a* and 4*d*–4*f* has a minor influence.

It must be underlined that a small change of restraints imposed on H atoms results in significantly different values of the dipole moment (especially for softer restraints on the ADPs). However, the best model predicted from the theoretical calculations, with additional restraints on H-atom ADPs,

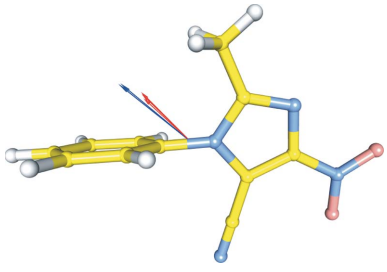

Figure 8
Dipole-moment directions in model 3. Blue: *a*–*c*; red: *d*–*f*.

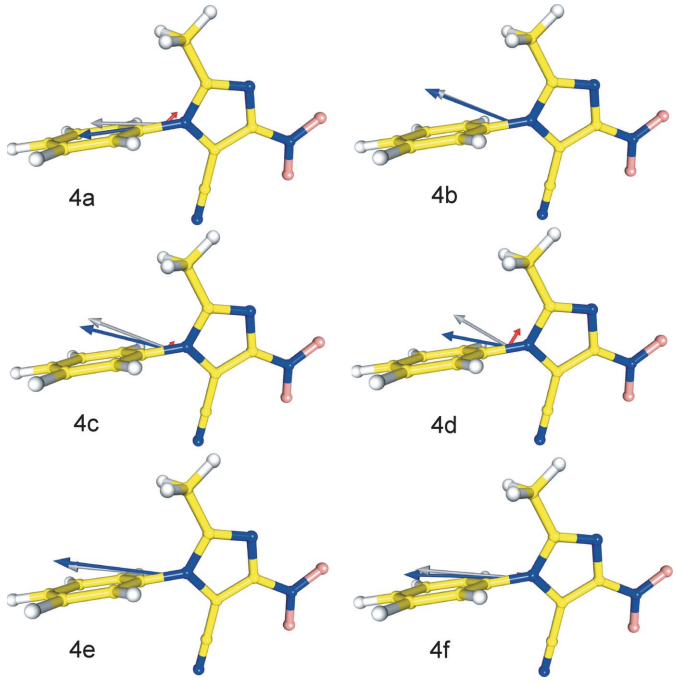

Figure 9
Dipole-moment vectors for the experimental multipolar models (grey, total; red, dipole moment using only atomic dipole contributions; blue, dipole moment using only atomic monopole charge contributions).

Table 6
Results of the VIR_{exp} refinement.

All results are given with an $I/\sigma(I) > 2$ cutoff for a reciprocal resolution up to $s = 1$ Å^{-1}. No. of reflections = 6164. The number of refined variables is 428. ModR: stereochemical restraints similar to VIR_{theo}, except for linearity ($\sigma_1 = 0.01$ Å), similarity of kappa for the Lp's of the nitro group are added. CER: chemical equivalence restraints are the same as in theoretical models and in MM_{exp}.

Model	Restraints	*RF*, *wR2F* (%)	Goof	Dipole moment μ (D)	μ with H-atom ADPs from *SHADE* not refined	Angle between μ_{theo} and μ_{calc} vectors
5*a*	ModR κ_{hyd} = 1.1 CER	3.062 2.737	1.22	9.02	*13.32*	43.4†/11.5‡
5*b*	ModR κ_{hyd} = 1.13 CER	3.064 2.740	1.22	9.94	*15.14*	31.7/11.1
5*c*	ModR κ_{hyd} = 1.16 CER	3.066 2.741	1.22	11.24	*17.03*	21.3/12.4
5*d*	ModR κ_{hyd} = 1.2 CER	3.094 2.794	1.25	13.03	*19.05*	21.1/12.8
5*e*	ModR κ_{hyd} = 1.1 CER	3.089 2.792	1.25	10.70	*12.77*	19.7/10.8
5*f*	ModR κ_{hyd} = 1.13 CER	3.094 2.797	1.25	12.31	*14.79*	15.7/11.4
5*g*	ModR κ_{hyd} = 1.16 CER	3.095 2.798	1.25	13.78	*16.34*	12.8/12.0
5*h*	ModR κ_{hyd} = 1.2 CER	3.101 2.806	1.25	16.17	*18.64*	10.8/14.1

† *SHADE* restraints. ‡ *SHADE* constraints.

gives a μ value of 11.1 D, in excellent agreement with the theoretical 10.6 D value, but a slightly different direction.

3.5.2. Virtual-atom model (VIR_{exp}). Two groups of models were tested in this section: 5*a*–5*d* with one virtual atom on N═O bonds and 5*e*–5*h* with the two atoms, even if not deemed necessary. The virtual-atom refinement seems to work well to account for the aspherical electron density fitted to experimental data, as shown on the residual maps (Fig. 10). The corresponding static maps are encouraging despite the unique type of virtual-atom scattering factor used to describe all the covalent bonds. The strategy for dipole-moment predictions cannot be estimated from theoretical structure-factor refinement, according to the VIR_{theo} model (see §3.2), the optimal κ_{hyd} for the correct magnitude and direction should be 1.13 and other constraints/restraints have no influence. This κ_{hyd} value led to slightly lower (5*b*) or higher (5*f*) μ values than expected in the case of experimental data; therefore other values were tested. Moreover, the influence of ADP values from *SHADE*, which was crucial in MM_{exp} refinements, was verified as well.

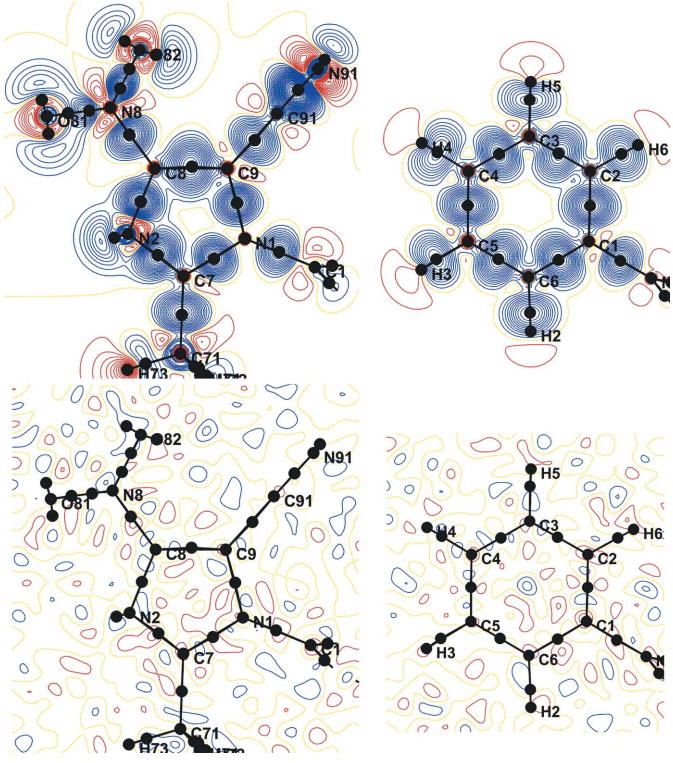

Figure 10
Static deformation and Fourier residual maps for model 5*f*; contours ±0.05 e A^{-3}, resolution up to $s = 1$ A^{-1}.

Eight different models with κ_{hyd} constrained to 1.1, 1.13, 1.16 and 1.2, with different treatments of the H-atom ADPs and single or double virtual atoms on the N═O bonds were tested. The μ dependence on the H-atom ADPs is clearly visible especially for models 5*a*–5*d* (Table 6) with a difference of more than 5 D; the difference is lower for models 5*e*–5*h* (2 D). Refinement 5*e* ($\kappa = 1.1$) with H-atom ADPs constrained by *SHADE* gives the best dipole moment in both magnitude and direction (Fig. 11).

The comparison of κ and P_{val} for the four models with different κ_{hyd} constraints shows that the most affected parameters are the H-atom valence populations and the κ and P_{vir} of the virtual atoms positioned on the X—H bonds. A possible improvement would be to define a new scattering factor for C—H virtual atoms.

3.5.3. Kappa model (KM_{exp}). The best kappa model from the theoretical calculation predictions is with κ_{hyd} restricted to the value 1.4, as recommended by Coppens *et al.* (1979).

Refining the charge density with the geometry from the best multipolar model (6*a*, Table 7) results in slightly higher dipole-

Table 7
Crystallographic statistics and dipole-moment moduli of the KM_{exp} refinement.

Cutoff $I/\sigma(I) > 2$ and reciprocal resolution up to $s = 1$ Å^{-1}. No. of reflections = 6164.

Model	Restraints/ constraints	κ_{hyd}	No. of variables	*RF*, *wR2F* (%)	Goof	μ (D)	Angle between μ_{theo} and μ_{calc} vectors
6*a*	restraints†	1.4	42	4.454 5.989	2.830	13.76	23.8
6*b*	restraints	refined ⟨1.21⟩	50	4.447 5.954	2.815	8.90	91.9

† Restraints on chemical similarity are the same as in KM_{theo}.

moment magnitude, but with a direction close to the expected one. In model 6*b*, no constraints were applied to κ_{hyd} ($\langle\kappa_{hyd}\rangle$ = 1.21). In this case, the magnitude of $\boldsymbol{\mu}$ is closer to the theoretical one, but its direction totally changes. The differences between the κ and P_{val} parameters of non-H atoms are negligible (except for C71 from the methyl group), whereas for H atoms the decrease of κ (13–17%) in model 6*b* is related to an increase of P_{val} (+18–23%; Fig. 12).

4. Conclusions

In this paper we have tried to achieve a thorough derivation of dipole moments from high-resolution X-ray diffraction refinement, as their estimation is by far the most difficult task, using theoretical and experimental structure factors.

Different electron-density models were tested (the kappa model, the multipolar model and the virtual-atom model) and it is shown that dipole moments (magnitude and direction) are extremely sensitive to the refinement strategy, in contrast to the topological analysis of the electron density: all models give the same topological properties (position, density and Laplacian at the critical point, bond paths . . .). The truthful refinement requires careful estimation of the H-atom positions and ADPs (neutron positions, anisotropy obtained by *SHADE*, no quadrupolar components) and leads to the right dipole moment in both multipole and virtual-atom models, but not in the kappa model.

Moreover, for the multipole electron-density modelling over-parametrization must be avoided as it can lead to wrong dipole populations because of an effective non-orthogonality of the restricted spherical harmonic basis set even if the least-squares residuals are slightly better. Therefore the H atoms should be refined up to dipoles, non-H atoms up to octupoles and non-H electron-rich atoms up to hexadecapoles, with the κ and κ' of H atoms restrained to 1.16 and 1.25, respectively.

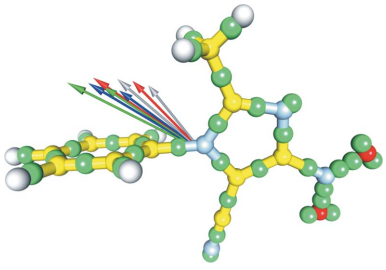

Figure 11
Dipole-moment vectors $\boldsymbol{\mu}$ in models 5*e*–5*h* (*e*, grey; *f*, blue; *g*, red; *h*, green) with ADP constraints (smaller angle to the Ph ring) and restraints (bigger angle to the Ph ring).

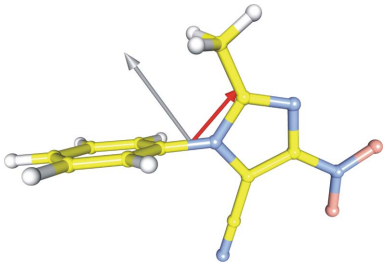

Figure 12
Dipole-moment vectors for the kappa models 6*a* (grey) and 6*b* (red).

This work was partially financed by grants from the Polish Ministry of Science and Education (grant Nos. N204 005136 and N204 028138) and the French Embassy in Warsaw within the framework of a cotutelle bursary for APP. We also thank Lorraine Université and CNRS for support.

References

Abramov, Y. A., Volkov, A. V. & Coppens, P. (1999). *Chem. Phys. Lett.* **311**, 81–86.
Afonine, P. V., Grosse-Kunstleve, R. W., Adams, P. D., Lunin, V. Y. & Urzhumtsev, A. (2007). *Acta Cryst.* D**63**, 1194–1197.
Afonine, P. V., Lunin, V. Y., Muzet, N. & Urzhumtsev, A. (2004). *Acta Cryst.* D**60**, 260–274.
Allen, F. H., Watson, D. G., Brammer, L., Orpen, A. G. & Taylor, R. (2006). *International Tables for Crystallography*, Vol. C, 1st online ed., ch. 9.5, pp. 790–811. Chester: International Union of Crystallography.
Bader, R. F. W. (1990). *Atoms in Molecules: a Quantum Theory*. Oxford: Clarendon Press.
Bąk, J. M., Domagała, S., Hübschle, C., Jelsch, C., Dittrich, B. & Dominiak, P. M. (2011). *Acta Cryst.* A**67**, 141–153.
Clementi, E. & Roetti, C. (1974). *At. Data Nucl. Data Tables*, **14**, 177–478.
Coppens, P. (1997). *X-ray Charge Density and Chemical Bonding*. New York: Oxford University Press.
Coppens, P., Abramov, Y., Carducci, M., Korjov, B., Novozhilova, I., Alhambra, C. & Pressprich, M. R. J. (1999). *J. Am. Chem. Soc.* **121**, 2585–2593.
Coppens, P., Guru Row, T. N., Leung, P., Stevens, E. D., Becker, P. J. & Yang, Y. W. (1979). *Acta Cryst.* A**35**, 63–72.
Dadda, N., Nassour, A., Guillot, B., Benali-Cherif, N. & Jelsch, C. (2012). *Acta Cryst.* A**68**, 452–463.
Dietrich, H., Scheringer, C., Meyer, H., Schulte, K.-W. & Schweig, A. (1979). *Acta Cryst.* B**35**, 1191–1197.
Domagała, S. & Jelsch, C. (2008). *J. Appl. Cryst.* **41**, 1140–1149.
Dovesi, R., Saunders, V. R., Roetti, C., Orlando, R., Zocovich-Wilson, C. M., Pascale, F., Civalleri, B., Doll, K., Harrison, N. M., Bush, I. J., D'Arco, Ph. & Llunell, M. (2010). *CRYSTAL09 User's Manual*. University of Turin, Turin, Italy.
Durka, K., Kamiński, R., Luliński, S., Serwatowski, J. & Woźniak, K. (2010). *Phys. Chem. Chem. Phys.* **12**, 13126–13136.
Guillot, B. (2011). *Acta Cryst.* A**67**, C511–C512.

Guillot, B., Viry, L., Guillot, R., Lecomte, C. & Jelsch, C. (2001). *J. Appl. Cryst.* **34**, 214–223.
Hansen, N. K. & Coppens, P. (1978). *Acta Cryst.* A**34**, 909–921.
Hariharan, P. C. & Pople, J. A. (1973). *Theor. Chim. Acta*, **28**, 213–222.
Hohenberg, P. & Kohn, W. (1964). *Phys. Rev. B*, **136**, 864–871.
Jelsch, C., Guillot, B., Lagoutte, A. & Lecomte, C. (2005). *J. Appl. Cryst.* **38**, 38–54.
Kubicki, M., Borowiak, T., Dutkiewicz, G., Souhassou, M., Jelsch, C. & Lecomte, C. (2002). *J. Phys. Chem.* B**106**, 3706–3714.
Le Page, Y. & Gabe, E. J. (1979). *J. Appl. Cryst.* **12**, 464–466.
Lee, C., Yang, W. & Parr, R. G. (1988). *Phys. Rev. B*, **37**, 785–789.
Madsen, A. Ø. (2006). *J. Appl. Cryst.* **39**, 757–758.
Moss, G. R., Souhassou, M., Blessing, R. H., Espinosa, E. & Lecomte, C. (1995). *Acta Cryst.* B**51**, 650–660.
Mullen, D. & Hellner, E. (1977). *Acta Cryst.* B**33**, 3816–3822.
Mullen, D. & Hellner, E. (1978*a*). *Acta Cryst.* B**34**, 1624–1627.
Mullen, D. & Hellner, E. (1978*b*). *Acta Cryst.* B**34**, 2789–2794.
Paul, A., Kubicki, M., Jelsch, C., Durand, P. & Lecomte, C. (2011). *Acta Cryst.* B**67**, 365–378.
Paul, A., Kubicki, M., Kubas, A., Jelsch, C., Fink, K. & Lecomte, C. (2011). *J. Phys. Chem. A*, **115**, 12941–12952.
Pérès, N., Boukhris, A., Souhassou, M., Gavoille, G. & Lecomte, C. (1999). *Acta Cryst.* A**55**, 1038–1048.
Pillet, S., Souhassou, M., Lecomte, C., Schwarz, K., Blaha, P., Rérat, M., Lichanot, A. & Roversi, P. (2001). *Acta Cryst.* A**57**, 290–303.
Scheringer, C. (1980). *Acta Cryst.* A**36**, 205–210.
Scheringer, C., Kutoglu, A., Mullen, D. & Hellner, E. (1978). *Acta Cryst.* A**34**, 475–476.
Scheringer, C., Mullen, D. & Hellner, E. (1978). *Acta Cryst.* A**34**, 621–625.
Scheringer, C., Mullen, D., Hellner, E., Hase, H. L., Schulte, K.-W. & Schweig, A. (1978). *Acta Cryst.* B**34**, 2241–2243.
Spackman, M. A. (1992). *Chem. Rev.* **92**, 1769–1797.
Spackman, M. A., Munshi, P. & Dittrich, B. (2007). *Chem. Phys. Chem.* **8**, 2051–2063.
Stewart, R. F., Davidson, E. R. & Simpson, W. T. (1965). *J. Chem. Phys.* **42**, 3175–3187.
Volkov, A., Abramov, Y. A. & Coppens, P. (2001). *Acta Cryst.* A**57**, 272–282.
Volkov, A., Gatti, C., Abramov, Y. & Coppens, P. (2000). *Acta Cryst.* A**56**, 252–258.